



# SYNTHESIS, CHARACTERIZATION AND ELECTRICAL STUDIES OF HAEMATITE ( $\text{Fe}_2\text{O}_3$ ) NANO PARTICLES PREPARED BY SOL GEL AUTO COMBUSTION METHOD

\*R. M. Belekar, \*S. D. Nagdive, #B. A. Shingade

Department of Physics and Electronics, Government Vidarbha Institute of Science and Humanities, Amravati, Maharashtra, India-444 604

#Department of Physics, Bhawabhuti Mahavidyalaya, Amgaon, Gondia, India.-441902

\*Corresponding Author Email: [rajubelekar@gmail.com](mailto:rajubelekar@gmail.com)

## Abstract

In the present work haematite ( $\text{Fe}_2\text{O}_3$ ) nanoparticles were synthesized using sol gel auto combustion method using solution combustion reaction between ferric nitrate as oxidizer and a mixture of urea and glycine fuel as reducer. In this fuel mixture, urea was taken as stoichiometric fuel and glycine was added as excess fuel to alter the exothermicity of redox reaction between ferric nitrate and urea. The synthesized powder were characterized by XRD, FT-IR, TGA-DTA showing that the powders were composed of polycrystalline oxides with crystallite size of 30 nm with gamma  $\text{Fe}_2\text{O}_3$  phase without sintering. The phase transition from gamma  $\text{Fe}_2\text{O}_3$  to alpha haematite occurs at temperature of  $482^\circ\text{C}$ . The curie temperature was calculated from Gouy's balance and found to be 250 K. The electrical conductivity of nano  $\text{Fe}_2\text{O}_3$  in pellet form was studied by impedance analyser at different temperature and frequencies. The variation of dielectric constant, ac conductivity with temperature and frequencies was also studied.

**Keywords:** Haematite, Mixed fuel approach, electrical conductivity.

## 1. Introduction:

Iron oxide is one of the transition metal oxide that commonly exists in three phases in nature: maghemite ( $\gamma\text{-Fe}_2\text{O}_3$ ), magnetite ( $\text{Fe}_3\text{O}_4$ ) and haematite ( $\alpha\text{-Fe}_2\text{O}_3$ ). These materials find wide applications in various fields because of their catalytic activity, biocompatibility, low-cost, nontoxicity and

environmentally friendly nature [1, 2].  $\text{Fe}_2\text{O}_3$ , the iron oxide has four crystallographic phases, namely maghemite ( $\gamma\text{-Fe}_2\text{O}_3$ ), haematite ( $\alpha\text{-Fe}_2\text{O}_3$ ), maghemite ( $\gamma\text{-Fe}_2\text{O}_3$ ),  $\beta\text{-Fe}_2\text{O}_3$  and  $\epsilon\text{-Fe}_2\text{O}_3$  [3]. Out of which haematite is the thermodynamically stable phase of  $\text{Fe}_2\text{O}_3$ , and it is the subject of this current research work. Haematite happens to be exists in the rhombohedral crystal system with n-type semiconducting properties [4]. Iron oxide ( $\alpha\text{-Fe}_2\text{O}_3$ ) has been studied in various fields, including applications in photocatalysis [5–8], pigments [9], gas sensors [10], solar cells [11], and lithium ion batteries [12]. The  $\gamma\text{-Fe}_2\text{O}_3$  undergoes a transformation to  $\alpha\text{-Fe}_2\text{O}_3$  above a transformation temperature ( $T_t$ ) (reported to be of  $500^\circ\text{C}$  for  $\gamma\text{-Fe}_2\text{O}_3$  NPs).

There is a homogeneous dispersion of nanoscale materials inside bulk thermoelectric matrices. [13]. The heat of transport/storage of materials is determined by phonons characteristics like frequency, scattering, velocity etc [14]. The boundaries of nanoparticles can acts as scattering centers for phonons transport which reduces their mean free path [15]. The result of which is reduction in its lattice thermal conductivity of nanomaterial. Thus the thermal conductivity of materials is reduced to improve their electric and magnetic properties for thermo-electric and thermo-magnetic applications. Because of low electrical conductivity, the electrical and chemical stability of nano scale material are also enhanced.

Among the available chemical processes, self-sustaining solution combustion synthesis is convenient in process, simple in

experimental device and time saving. Solution combustion synthesis process involves an aqueous mixture containing suitable metal salts which are the precursors of the final desired oxide and a proper sacrificial organic fuel which acts as reagent reducer. Generally, hydrate nitrates are preferred to other salts because of their good solubility in water which allows them to obtain a highly homogeneous solution. Urea is the most convenient fuel that can be used in the combustion processes [16] because of its relatively low price, availability, commercially grade and safety. In this study, haematite ( $\text{Fe}_2\text{O}_3$ ) nanoparticles were synthesized using sol gel auto combustion method using solution combustion reaction between ferric nitrate as oxidizer and a mixture of urea and glycine fuel as reducer. The synthesized powder will be characterized by XRD, FT-IR, TGA-DTA and electrical and magnetic studies will also be conducted.

## 2. Experimental:

The precursor involved in this synthesis is ferric nitrate ( $\text{Fe}(\text{NO}_3)_3 \cdot 9\text{H}_2\text{O}$ ) from Merck (AR Grade). Urea  $\text{CO}(\text{NH}_2)_2$  and glycine ( $\text{C}_2\text{H}_5\text{NO}_2$ ) are used as fuel because of its relatively low price, availability, commercially grade and safety. The stoichiometric quantities of the oxidizers ( $\text{Fe}(\text{NO}_3)_3 \cdot 9\text{H}_2\text{O}$ ) and fuels (Urea and glycine) were mixed in 50 ml deionized water with constant stirring. In this reaction urea was taken as stoichiometric fuel and glycine was added as excess fuel to alter the exothermicity of redox reaction between ferric nitrate and urea. The solution was then kept on hot plate in order to evaporate more than half of water content. This solution moved to microwave with power of 900 Watt. After some minutes, first a gel-like structure was obtained and then swelled, followed by the evolution of a large volume of gases. In other word self propagating solution combustion occurred. This reaction product was treated at temperature of  $500^\circ\text{C}$  to obtain desired phase of  $\text{Fe}_2\text{O}_3$ . The identification and phase determination of the compound were done by powder XRD technique and other

characterization were also be done with FT-IR, TGA-DTA.

For the preparation of pellets, all the compounds are grinded separately to fine particles in an agate mortar. The powder is then mixed with solution of 5% polyvinyl acetate (PVA) in A.R. grade acetone, which serves as a binder. About 2ml of binder per gram of powder is sufficient to give well-molded pellets. The plastic mass formed by mixing binder in the powdered sample is then pressed in a hydraulic press under a pressure of 50-tones/sq. inch for about fifteen minutes. The pellets so formed are heated in a furnace up to  $400^\circ\text{C}$  for about 3 hour to remove the binder. The furnace is then cooled to the room temperature by a natural way to obtain crack and moisture free hard pellets. The end faces of pellets are gently grinded with acetone to ensure its smooth face. After formation of pellets, a thin layer of silver paste is applied on both the surfaces of the pellets to provide good electrical contacts. The contacts are dried up to obtained a thin layer of silver which is adherent and chemically inert. The contacts are conformed, before the experimental study. The dimensions of pellets are measured accurately using digital vernier calliper.

## 3. Results and Discussion:

The prepared samples of  $\text{Fe}_2\text{O}_3$  were examined with the help of X ray diffraction technique in order to study the haematite phase and to determine particle size [17]. Figure 1 shows the x-ray diffraction (XRD) peak lines from the standard order diffraction files of  $\alpha\text{-Fe}_2\text{O}_3$  (33-0664), and  $\gamma\text{-Fe}_2\text{O}_3$  (39-1346), and it can be found that  $\gamma\text{-Fe}_2\text{O}_3$  has a crystal structure similar to that of  $\text{Fe}_3\text{O}_4$ . [18] It is noteworthy that the annealing treatment is a key step in most synthesis of different crystalline phase of iron oxides. Any type of iron oxide can be obtained from the other types by oxidizing or reducing in the annealing treatment. It is also clear that the annealing temperature was not sufficient to turn  $\gamma\text{-Fe}_2\text{O}_3$  into  $\alpha\text{-Fe}_2\text{O}_3$ , as some unidentified peaks appeared in X-ray diffractogram.

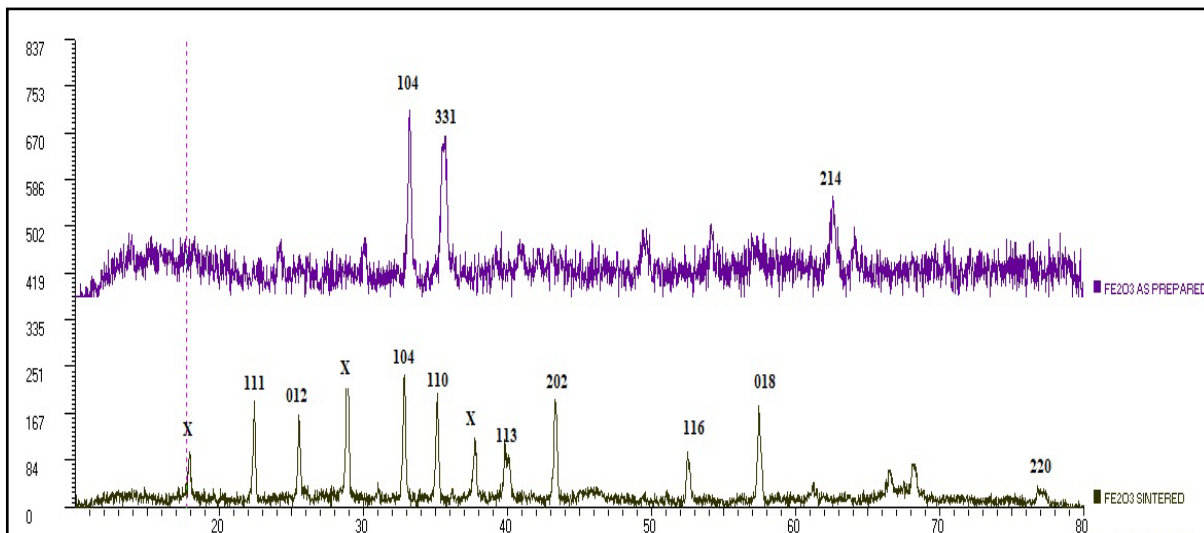


Figure 1: XRD diffractogram of nano  $\text{Fe}_2\text{O}_3$  as prepared and sintered sample with JCPDS Card No. 39-1346 and 33-0664 respectively.

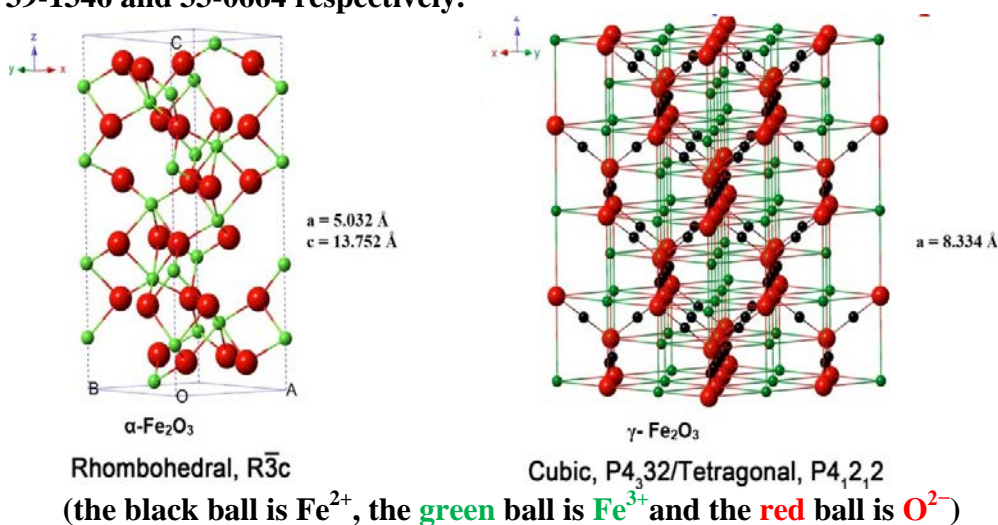


Figure 2: Crystal Structure of nano  $\text{Fe}_2\text{O}_3$  in rhombohedral and cubic form.

As shown in figure 2, the structure of  $\gamma\text{-Fe}_2\text{O}_3$  is cubic; each unit of  $\gamma\text{-Fe}_2\text{O}_3$  contains 32  $\text{O}^{2-}$  ions,  $21\frac{1}{3}$   $\text{Fe}^{3+}$  ions and  $2\frac{1}{3}$  vacancies. Oxygen anions give rise to a cubic close-packed array while ferric ions are distributed over tetrahedral sites (eight Fe ions per unit cell) and octahedral sites (the remaining Fe ions and vacancies). Therefore,  $\gamma\text{-Fe}_2\text{O}_3$  can be considered as fully oxidized magnetite, and it is an n-type semiconductor with a bandgap of 2.0 eV.  $\alpha\text{-Fe}_2\text{O}_3$  is an n-type semiconductor with a band gap of 2.3 eV, where the conduction band (CB) is composed of empty d-orbitals of  $\text{Fe}^{3+}$  and the valence band (VB) consists of occupied 3d crystal field orbitals of  $\text{Fe}^{3+}$  with some admixture from the O 2p non-bonding orbitals [19]. As shown in figure 2,  $\text{Fe}^{3+}$  ions occupy two-thirds of the octahedral sites that are confined by the nearly ideal hexagonal close-packed O lattice.

The infrared spectra of the as-synthesized precursor samples before thermal treatment and after thermal treatment at  $500^\circ\text{C}$  is shown in figure 3. The prominent bands at  $602\text{ cm}^{-1}$  and  $465\text{ cm}^{-1}$  observed in the spectrum (Fig. 3) which can be attributed to Fe-O vibrational modes. [20-22]. The peak observed at  $1670\text{ cm}^{-1}$  attributed to O-H bending vibrational modes. [23,24]. This strong band may also be due to physically adsorbed water. Although the O-H bond vibration around  $3000\text{ cm}^{-1}$  is still present, the intensity of this band decreased markedly on heating the samples at  $500^\circ\text{C}$ . The prominent band at  $1031\text{ cm}^{-1}$  can be assigned to the absorption of -C-O-C bonds. The band at  $1370\text{ cm}^{-1}$  may be attributed to -C-O stretching mode. [25] Absorption at  $1409\text{ cm}^{-1}$  should be attributed to C-H vibration of the hydrolyzed products.

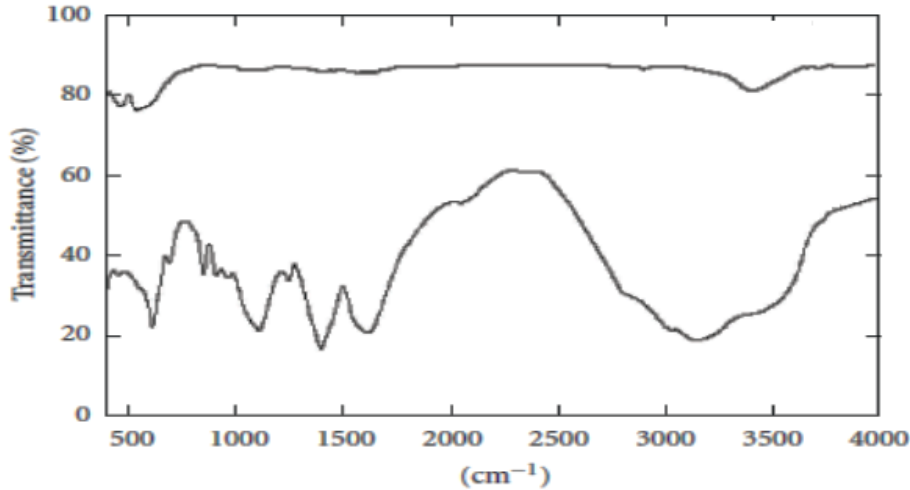


Figure 3 FT-IR spectrum of nano Fe<sub>2</sub>O<sub>3</sub> as prepared and treated at 500°C.

The temperature dependence of magnetic susceptibility measurement was done by using Gouy’s Balance method. The plots of the inverse of magnetic susceptibility ( $1/\chi$ ) versus temperature for  $Fe_2O_3$  samples are shown in Fig. 4. The value of inverse of magnetic susceptibility ( $1/\chi$ ) increases with enhancement in temperature in the ferromagnetic region followed by a sudden increase at the certain temperature representing transition to the paramagnetic region. The temperature at which the magnetic transition occurs is known as the Curie temperature ( $T_c$ ). The values of Curie

temperature ( $T_c$ ) are calculated by extrapolating the paramagnetic region to the X-axis. Low temperature magnetic transition occurs at 250 K (Morin temperature). At temperature  $T \leq 250$  K: The magnetic arrangement has  $Fe^{3+}$  spins directed along the [111] axis and paired across the shared octahedral face. At  $T \geq 250$  K: The spins become essentially localized in (111) sheets directed towards the three nearest neighbours. However, the spins have canted slightly out of the plane, giving rise to a weak ferromagnetic moment along the [111] axis.

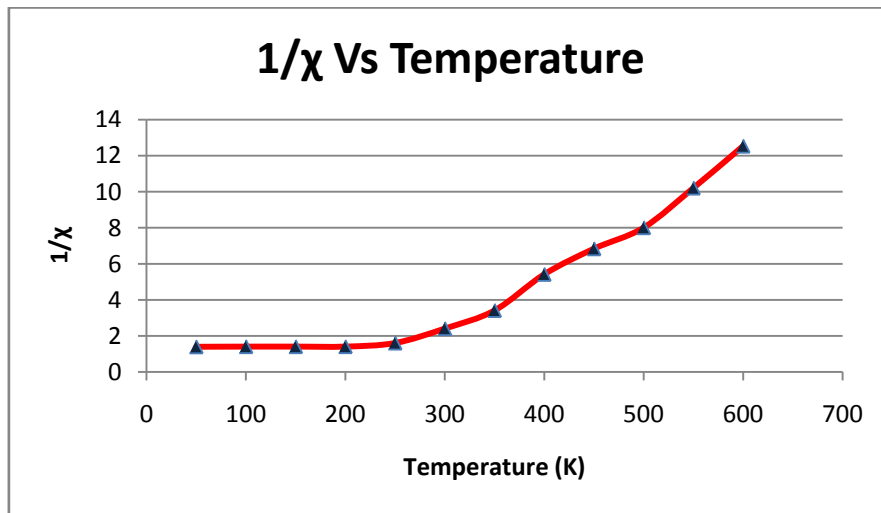


Figure 4: Plot of inverse susceptibility versus temperature.

The relationship between conductivity and temperature may be expressed as by the relation [1],

$$\sigma = \sigma_0 \exp\left(\frac{\Delta E}{KT}\right) \quad \text{-----} \quad (1)$$

Where,  $\sigma$  is the conductivity,  $T$  is the temperature,  $K$  is the Boltzmann constant, and  $\Delta E$  is the activation energy, is the energy

required to jump an electron to neighboring ion, so giving rise to electrical conductivity. The conductivity is measured by taking sample in the pellet form by Precision Impedance Analyzers 6500B Series.

Generally the  $Fe_2O_3$  are insulator at room temperature and act as a semiconductor under the influence of high temperature. The electrical conduction in  $Fe_2O_3$  is a combination

of electronic and ionic conduction such that conduction at low temperatures is dominated by electrons whereas at high temperature it is dominated by ionic hopping mechanism [27].

The electrical properties of the ferrite can be understood from the measurement of electrical conductivity, dielectric behaviour, thermoelectric power, etc. The mobility of charge carriers are the key quantities for obtaining inner details of conductivity. The low conductivity of ferrite greatly influences the various applications at microwave frequencies. The ferrite and ferroelectric can have their own electrical properties but their composites with different substitutions of divalent, trivalent and tetravalent ions are designed to give more effective property. Though ferrites are semiconductors at high temperature, the conduction mechanism is quite different than

that of semiconductors. In ferrites the carrier concentration is almost constant but mobility of carriers is affected by temperature. Thus, the conduction in ferrites can be explained in terms of polaron hopping process and there are experimental evidences for the existence of polarons and its hopping [28,29].

The plots of log conductivity ( $\sigma$ ) with inverse of temperature for  $\text{Fe}_2\text{O}_3$  are shown in **fig.5**. From these plots it can be seen that the conductivity increase slowly up to a certain temperature called as transition temperature ( $T_t$ ), where there is a slight change in slope occur after which a rapid increase is obtained. Above the transition temperature, the synthesized ferrite samples exhibit paramagnetic nature where it has disordered character.

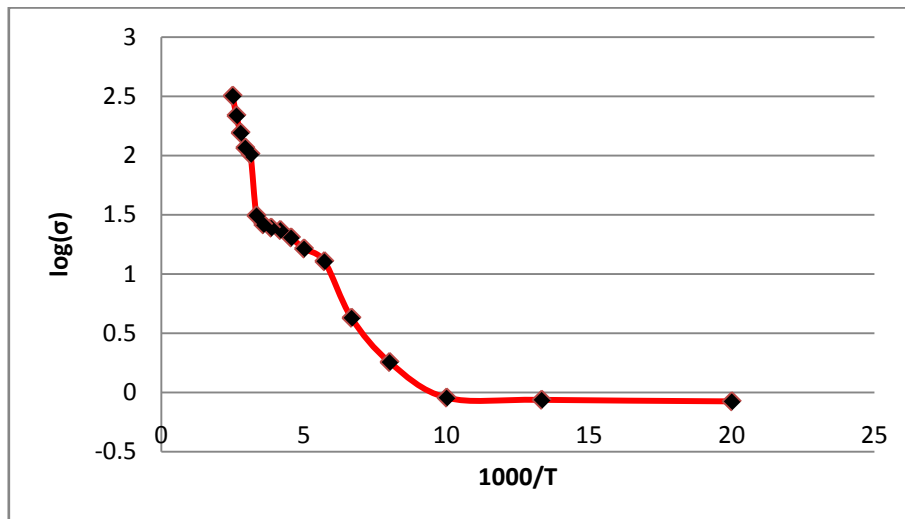


**Figure 5 :**Plot of  $\log(\sigma)$  versus  $1000/T$  for  $\text{Fe}_2\text{O}_3$  pellet

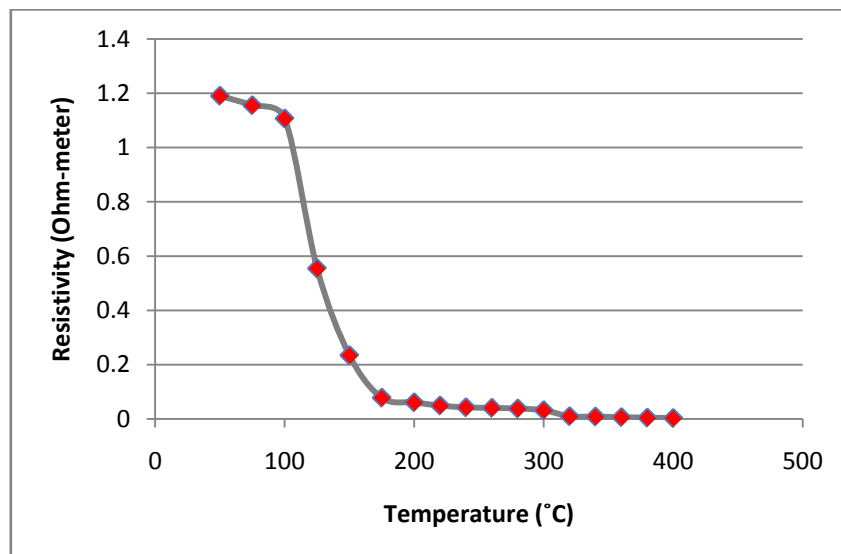


**Figure 6:** Plot of resistivity (in ohm-meter) versus temperature.



The electrical conductivity in ferrite is mainly due to hopping of electrons between ions of the same element present in more than one oxidation state, distributed randomly over crystallographically equivalent lattice sites. As the temperature is increased from 150 to 500°C, one can see that the electrical resistivity

decreases linearly as shown in figure 6, with an activation energy of  $1.68 \times 10^{-19}$  J (1.05 eV). Note that the conductivity at 500°C is higher than that of RT by about three orders of magnitude and by six orders of magnitude as compared with that at about 150°C.

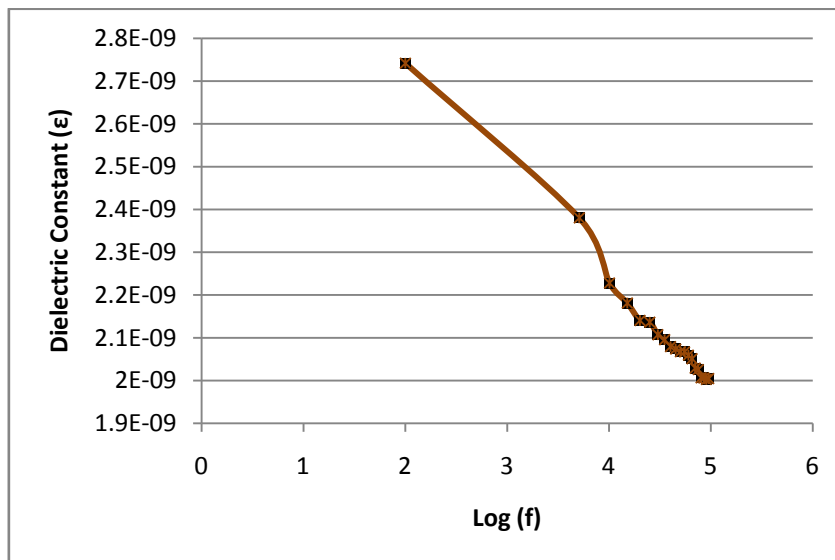


**Figure 7: Plot of dielectric constant versus log of frequency.**

The variation of dielectric constant with frequency for  $\text{Fe}_2\text{O}_3$  shown in the figure 7. It is seen that, the synthesized sample show frequency dependent phenomena i.e. the dielectric constant decreases with increasing frequency and then reaches to constant value. It is observed that  $\epsilon'$  decrease with increasing the applied field frequency showing a normal dielectric behavior of ferrites, which exists in non-homogenous layered structure of ceramic materials as explained by Maxwell–Wagner’s two-layer model [117, 118]. According to this model, ferrites consist of perfectly conducting grains separated by insulating grain boundaries, which offer hindrance to the conduction process. Under the influence of an applied field, displacement of charge carriers takes place. If resistance of grain boundary is large, the charge carriers align themselves at the grain boundaries, resulting in the polarization of the dielectric medium that leads to a large dielectric constant. As the frequency increases, the increase in electrical resistance due to dopant substitution diminishes the probability of charge carriers to reach the grain boundaries. This disrupts the polarization buildup in material leading to decrease the dielectric constant at higher frequencies.

From figure 7, it is seen that  $\epsilon'$  decreases gradually with increasing  $f$ . Such a behavior was previously reported for different ferrites [30,31] and could be explained assuming that the dielectric constant  $\epsilon'$  and the conductivity have the same origin where the conduction occurs through the electron hopping between  $\text{Fe}^{2+}$  and  $\text{Fe}^{3+}$  ions on the octahedral sites. By increasing the frequency, the electron hopping cannot follow the electric field fluctuations causing the dielectric constant  $\epsilon'$  to decrease as we found experimentally. According to Koops’s model [32] the dielectric constant at low frequency comes from the grain boundaries which have a high dielectric constant due to high resistivity at grains boundaries. At high frequency  $\epsilon'$  results from the grains which have a small dielectric constant due to low resistivity. The higher values of dielectric constant at low frequency are due to the voids, dislocations and other defects. High dielectric constant decreases the penetration depth of the electromagnetic waves by increasing the skin effect. Hence, the much lower dielectric constants obtained for the ferrites warrant their application at high frequencies [33].

#### 4. Conclusion:

The nano  $\text{Fe}_2\text{O}_3$  sample was successfully prepared by simple solution

combustion synthesis method using the precursors iron nitrate and urea as fuel. The structure and phase determination was carried out by XRD analysis. The X-ray diffraction of the prepared sample has shown a cubic structure indicating an amorphous  $\gamma$ -Fe<sub>2</sub>O<sub>3</sub> phase with an average crystalline size of 32 nm calculated from the Scherrer formula. When the sample is treated at some elevated temperature of 500°C,  $\gamma$ -Fe<sub>2</sub>O<sub>3</sub> is converted into thermodynamically stable  $\alpha$ -Fe<sub>2</sub>O<sub>3</sub> as indicated by XRD. The sharp peaks in the XRD of the sintered sample indicated the crystalline nature of  $\alpha$ -Fe<sub>2</sub>O<sub>3</sub>. When the sample is prepared by solution combustion synthesis it requires less temperature to form the stable alpha phase ( $\alpha$ -Fe<sub>2</sub>O<sub>3</sub>). The structural formation of ferrite was also confirmed by FTIR Spectra, showing band ranges 602 cm<sup>-1</sup> and 465 cm<sup>-1</sup> corresponding to Fe-O vibrations. It is also clear that if one wishes to obtain  $\gamma$ -Fe<sub>2</sub>O<sub>3</sub> by calcination of the  $\gamma$ -FeOOH gel, annealing at a lower temperature must be employed. The temperature dependence of electrical conductivity shows that the electrical conductivity of sintered Fe<sub>2</sub>O<sub>3</sub> at 500 °C is three orders of magnitude higher than that of RT. In addition, the dominant charge carriers are found to be holes in the range between RT and 380°C, while electrons above 380°C according to the Seebeck measurement. The combined inductive and capacitive nature in the composites is a promising candidate for design simplification and size minimization of many passive electronic devices such as integrated filters and microwave absorbers. The AC conductivity of composites increases with increase in frequency, this is due to hopping of charge carriers amongst localized sites. The relative susceptibility gradually increases up to blocking temperature, suggestive of single domain (SD) existence in majority in ferrite phase.

## REFERENCES

- [1] G.K. Mor, H.E. Prakasam, O.K. Varghese, K. Shankar, C.A. (2007) Grimes, *Nano Lett.* 7, 2356–2364
- [2] S.M. El-Sheikh, F.A. Harraz, K.A. Saad, (2009) *J. Alloys Compd.* 487, 716–723
- [3] S. Sakurai, A. Namai, K. Hashimoto, S. Ohkoshi, (2009) *J. Am. Chem. Soc.* 131, 18299–18303
- [4] A.S. Teja, P.Y. Koh, Prog. (2009), *Cryst. Growth Charact. Mater.* 55, 22–45
- [5] M. Mishra, D.M. Chun, (2015) *Appl. Catal. A* 498, 126–141.
- [6] S. Boumaza, A. Boudjemaa, S. Omeiri, R. Bouarab, A. Bouguelia, M. Trari, (2010) *Sol. Energy* 84, 715–721
- [7] Maneesha Mishra, Doo-Man Chun, *Applied Catalysis A: General*, Volume 498, 5 June 2015, Pages 126–141
- [8] Wei Chang, Maojin Zhang, Xiaosai Ren, Andrew Miller, (2017) *S. Afr. J. Chem. (Online)* vol.70 Durban
- [9] [Liliya Frolova](#), [Alexander Pivovarov](#), [Tatyana Butyrina](#), (2017) *Pigment & Resin Technology*, Vol. 46 Issue: 5, pp.356–361, <https://doi.org/10.1108/PRT-07-2016-0073>
- [10] Hung, Chu Manh, Hoa, Nguyen Duc, Van Duy, Nguyen, Van Toan, Nguyen, Le, Dang Thi Thanh, Van Hieu, Nguyen, *Journal of Science: Advanced Materials and Devices*, Volume 1, Issue 1, March 2016, Pages 45–50
- [11] S. Shinde, S. & Bansode, Rohit & Bhosale, Chandrakant & Rajpure, Keshav. (2011), *Journal of Semiconductors*. 32. 013001, doi:10.1088/1674-4926/32/1/013001.
- [12] Reddy, M V & Yu, Ting & Sow, C. H. & Xiang Shen, Ze & Lim, C.T. & V. Subba Rao, G & Chowdari, B. V. R.. (2007).  $\alpha$ -Fe<sub>2</sub>O<sub>3</sub>, 17. 2792 – 2799, doi: 10.1002/adfm.200601186
- [13] Kim W (2015) *J. Mater. Chem. C* 3 10336–48
- [14] Toberer E S, Baranowski L L and Dames C (2012) *Advances in thermal conductivity Ann. Rev. Mater. Res.* 42 179–209
- [15] Jeżowski A, Mucha J, Pazik R and Streck W (2007), *Appl. Phys. Lett.* 90 114104–7
- [16] K. Tahmasebi, M. Paydar, (2008) *J. Materials Chemistry and Physics* 109, 156–163
- [17] Tang, Z. X., C. M. Sorensen, K. J. Klabunde and G.C. Hadjipanayis (1991). *J. App. Phys.* 69(8):5279–5281
- [18] Martínez G, Malumbres A, Mallada R, Hueso J, Irusta S, Bomati-Miguel O and Santamaría (2012), *J. Nanotechnology*, 23, 425605.
- [19] Zhang Z, Boxall C and Kelsall G H (1993) Photoelectrophoresis of colloidal iron oxides: 1. Hematite (&agr;-Fe<sub>2</sub>O<sub>3</sub>) *Colloids Surf. A* 73 145
- [20] B. Pal, M. Sharon, *Thin Solid Films*, (2000), 379, 83–88.
- [21] Y.Y. Xu, D. Zhao, X.J. Zhang, W.T. Jin, P. Kashkarov and H. Zhang, *Physica E*, (2009), 41 806–811

- [22] E. Darezereshki, *Mater. Lett.*, (2011), 65, 642–645.
- [23] S.K. Apte, S.D. Naik, R.S. Sonawane and B.B. Kalew, *J. Am. Ceram. Soc.*, (2007), **90**, 412–414.
- [24] L. Song, S. Zhang, B. Chen, J. Ge and X. Jia, *Colloids Surf. A: Physicochem. Eng. Aspects*, (2010), **360**, 1–5.
- [25] S.S. Shankar, A. Rai, A. Ahmad and M. Sastry, *J. Colloid Interface Sci.*, (2004), **275**, 496–502.
- [26] Verwey E. J. W and Heilman, (1947) *J. Chem. Phys.*, **15**, 174.
- [27] M V Patrakeev, E B Mitberg, I A Leonidov, V L Kozhevnikov, (2001), *Sol. State. Ioni.*, **139**, 325–330.
- [28] Klinger M. I., (1975) *J. Phys. C. (G13)* **1**, (21), 3395.
- [29] Om Prakash, Mandal K. D., Christopher C. C., Sastry M. S. and Devendrakumar, (1994) *Bull Mater. Sci.*, **17**, 253.
- [30] J. C. Maxwell, *Electricity and Magnetism*, (1929) ,vol.1, Oxford University Press, Oxford, section 328.
- [31] K. W. Wagner, *Ann. Phys.* 40 (1913) 817.
- [32] C. Koop's, *Phys. Rev.* 83 (1951) 121.
- [33] V. N. Dhage, M. L. Mane, A. P. Kecha, C. T. Birajdar, K. M. Jadhav, *Physica B* (2011) 406, 789-793.